Int. J. Electrochem. Sci., 6 **(2011)** 6275 - 6289

International Journal of
ELECTROCHEMICAL
SCIENCE
www.electrochemsci.org

The Correlation between Electrochemical Corrosion Resistance and Mechanical Strength of As-Cast Al-Cu and Al-Si Alloys

Wislei R. Osório[1,2,*], *Claudio A. Siqueira*[3], *Carlos A. Santos*[4], *Amauri Garcia*[2]

[1] School of Applied Sciences / FCA, University of Campinas, UNICAMP, Campus Limeira, 1300, Pedro Zaccaria St. , Jd. Sta Luiza, 13484-350 Limeira, SP, Brazil
[2] Department of Materials Engineering, University of Campinas, UNICAMP, P.O. Box 6122, 13083–970 Campinas, SP, Brazil
[3] Department of Materials Engineering, Technology Centre, Federal University of Paraíba, UFPB, 58051-900 João Pessoa, PB, Brazil
[4] Pontifical Catholic University of Rio Grande do Sul – PUCRS, Faculty of Engineering, 90619-900 Porto Alegre, RS, Brazil
[*]E-mail: wislei@fem.unicamp.br

Received: 2 September 2011 / *Accepted:* 27 October 2011 / *Published:* 1 December 2011

The aim of the present work is to investigate the influence of solidification thermal parameters on the microstructural array of Al 5 wt.% Cu and Al 9 wt.% Si alloys castings with a view to developing correlations between the as-cast dendritic microstructure, the electrochemical corrosion resistance and the tensile mechanical strength. Considering the as-cast Al 5 wt.% Cu alloy, it was found that smaller secondary dendrite arm spacings (λ_2) increase both the ultimate tensile strength (UTS) and the corrosion resistance. For the Al 9 wt.% Si alloy, it is shown that the UTS also increase with the decrease in λ_2, however, the corrosion resistance decreases. A combined plot of corrosion resistance and UTS as a function of λ_2 is proposed with a view to determining an optimum range of secondary dendrite arm spacings which provides good balance between both properties.

Keywords: Aluminum alloys, dendritic microstructure, mechanical strength, electrochemical corrosion resistance.

1. INTRODUCTION

The primary advantage of aluminum alloys castings in general is a relatively high strength-to-weight ratio. They also exhibit other useful properties such as good resistance to certain types of corrosion and high electrical and thermal conductivity [1]. Mechanical properties of Al-Cu alloys depend on copper content. Copper is added to aluminum alloys to increase their strength, hardness,

fatigue and creep resistances and machinability [1]. The first and most widely used aluminum alloys are those containing 4 to 10 wt% Cu. However, of the main aluminum alloys, Al-Cu alloys have the lowest negative potential of corrosion. Copper generally reduces resistance to general corrosion and, in specific compositions and material conditions, stress corrosion susceptibility [1].

Al-Si alloys with silicon as a major alloying element constitute a class of material, which provides the most significant part of all shaped castings manufactured, especially in the aerospace and automotive industries [2]. This is mainly due to the outstanding effect of silicon in the improvement of casting characteristics, combined with other physical properties such as mechanical properties and corrosion resistance. In general, an optimum range of silicon content can be assigned to casting processes. For slow cooling rate processes (sand, plaster, investment) the range is 5 to 7 wt%, for permanent molds 7 to 9% and for die castings 8 to 12% [1-2].

Both Al-Cu and Al-Si alloys have been widely applied for many decades in components such as fuselages, wing skins and bulkheads (aerospace industry) and in combustion engines and cylinder liners (automotive industry) [1-3].

The effect of microstructure on metallic alloys properties has been highlighted in various studies and particularly, the influence of dendrite arm spacing upon the mechanical properties, i.e., ultimate tensile strength and yield strength, has been reported [4-10]. Recently, a number of studies have also focused on microstructure arrangement and corrosion behaviour relationships [11-15].

Although the metallurgical and micromechanical aspects of the factors controlling microstructure, unsoundness, strength and ductility, and corrosion resistance of as-cast alloys are complex, it is well known that solidification processing variables are of high order of importance. The cooling rate during solidification defines the fineness of the dendritic network. The solute redistribution, the anodic or cathodic electrochemical behaviour of each component of the alloy and the scale of dendrite spacings are the three main microstructural characteristics affecting the corrosion resistance of castings [11-15].

The present article focus on the influence of solidification cooling rate on the microstructural formation of both Al 5 wt% Cu and Al 9 wt% Si alloys castings and on the interrelation of the scale of the dendritic microstructure array, the mechanical strength and the corrosion resistance.

2. EXPERIMENTAL

2.1 Solidification experiments and metallography

The Al 5 wt.% Cu and Al 9 wt.% Si alloys samples were prepared from commercially pure (c.p.) Al (99.97 wt.%), electrolytic grade Cu (99.991wt.%) and Si (99.7 wt.%). The mean impurities detected in these c.p. metals are shown in Table 1.

Table 1. Chemical compositions of Al, Cu and Si used to prepare the alloys

Element (wt.%)	Cu	Fe	Pb	Si	Other
Copper (Cu)	99.991	0.015	0.012	0.003	<0.001
Aluminum (Al)	99.97	0.095	<0.002	0.19	<0.001
Silicon (Si)	99.71	0.12	<0.001	0.17	<0.001

The alloys were previously prepared in an electric resistance-type furnace and then stirred, degassed and poured into the casting chamber of a directional solidification set-up, which is shown in Fig. 1. It was designed in such way that heat is extracted only through the water-cooled bottom, promoting vertical upward directional solidification. The stainless steel cylindrical casting chamber had an internal diameter of 50 mm, a height of 110 mm and a wall thickness of 3 mm. The side walls were covered with a layer of insulating alumina to minimize radial heat losses. The bottom part of the mold was closed with a thin (3 mm thick) carbon steel sheet, which physically separates the metal from the cooling fluid. The temperatures were monitored via type J thermocouples and the temperature data were acquired automatically by a data acquisition system.

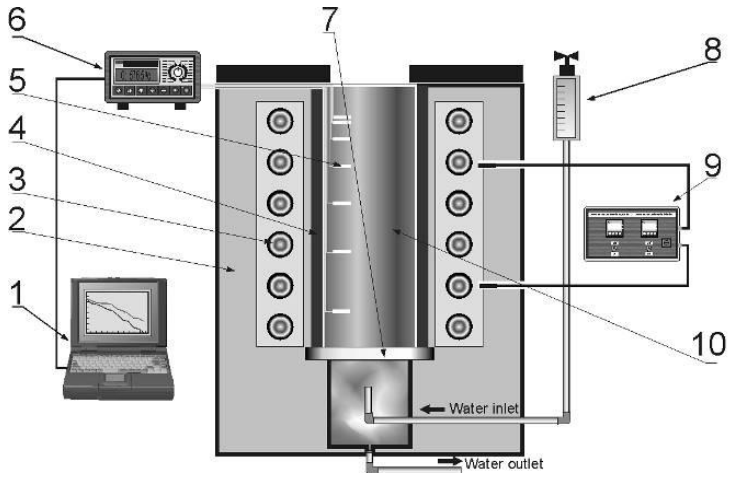

Figure 1. Schematic representation of the experimental solidification setup: 1) computer and data acquisition software; 2) insulating ceramic shielding; 3) electric heaters; 4) casting chamber; 5) thermocouples; 6) data logger; 7) heat-extracting bottom; 8) water flow meter; 9) temperature controller; 10) casting.

All specimens were prepared by conventional metallographic techniques. The specimens were etched with a solution of 0.5% HF in distilled water and a mixture of 15 mL HF, 4.5 mL HNO_3, 9 mL HCl, and 271.5 mL H_2O were used to reveal the microstructure and the macrostructure, respectively. Image processing systems Neophot 32 (Carl Zeiss, Esslingen, Germany) and Leica Quantimet 500 MC (Leica Imaging systems Ltd, Cambridge, England) were used to measure the secondary dendrite arm

spacings and their distribution range. The dendritic spacing was measured on the longitudinal section of the samples by averaging the distance between adjacent side branches.

2.2 Tensile testing

Fig. 2 shows a schematic representation of the specimens for the tensile tests and the position from where they were extracted along the casting length. These specimens were prepared according to specifications of ASTM Standard E 8M/04 and tested in a MTS Test Star II machine at a strain rate of $1x10^{-3}$ s^{-1} in the elastic range and of $4x10^{-3}$ s^{-1} in the plastic range. In order to ensure reproducibility of the tensile results, three specimens were tested for each selected position. The yield (0.2 % proof stress -YS) and ultimate tensile (UTS) strengths have been determined at different positions along the casting length.

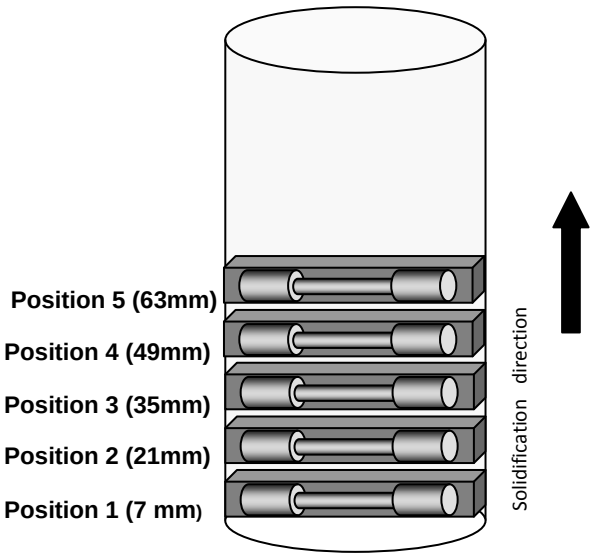

Figure 2. Schematic representation of positions from the casting bottom from where the specimens for tensile tests were extracted.

2.3 Polarization tests

Al-Cu and Al-Si alloy samples for corrosion tests were extracted longitudinally from the casting, at the same positions where samples were also removed for tensile testing, as depicted in Fig 2 (except at position P3).

These samples were adequately positioned at the glass corrosion cell kit, leaving a circular 1 cm^2 metal surface in contact with the naturally aerated and stagnant electrolyte (0.5 M NaCl solution at 25^{o}C (± 2 ^{o}C) and with neutral pH (6.85 ±0.25)). The samples were further ground up to a 1200 grit SiC finish, followed by distilled water washing and air drying before all electrochemical impedance spectroscopy (EIS) tests. A potentiostat (EG & G Princeton Applied Research, model 273A), a glass

corrosion cell kit with a platinum counter-electrode and a saturated calomel reference electrode (SCE) were used to perform the corrosion tests.

Potentiodynamic tests were also carried out in a 0.5 M NaCl solution at room temperature using a potentiostat. These tests were conducted by stepping the potential at a scan rate of 0.1667 mV s^{-1} from -900 to -500 mV (SCE) at open-circuit and duplicate tests were carried out.

3. RESULTS AND DISCUSSION

3.1 Resulting microstructure

Fig. 3 shows the secondary dendrite arm spacing (λ_2) as a function of cooling rate ($\dot{T}$) and tip growth rate (V_L) for both Al- 5 wt% Cu and Al- 9 wt% Si alloys. It can be observed that, as expected, λ_2 increases due to the decrease in cooling rate with increasing distance from the bottom of the casting [8-10, 16-18].

The microstructure of the as-cast Al-Cu alloy consists of an Al-rich dendritic matrix with a lamellar eutectic mixture in the interdendritic region formed by Al_2Cu particles and the Al-rich phase.

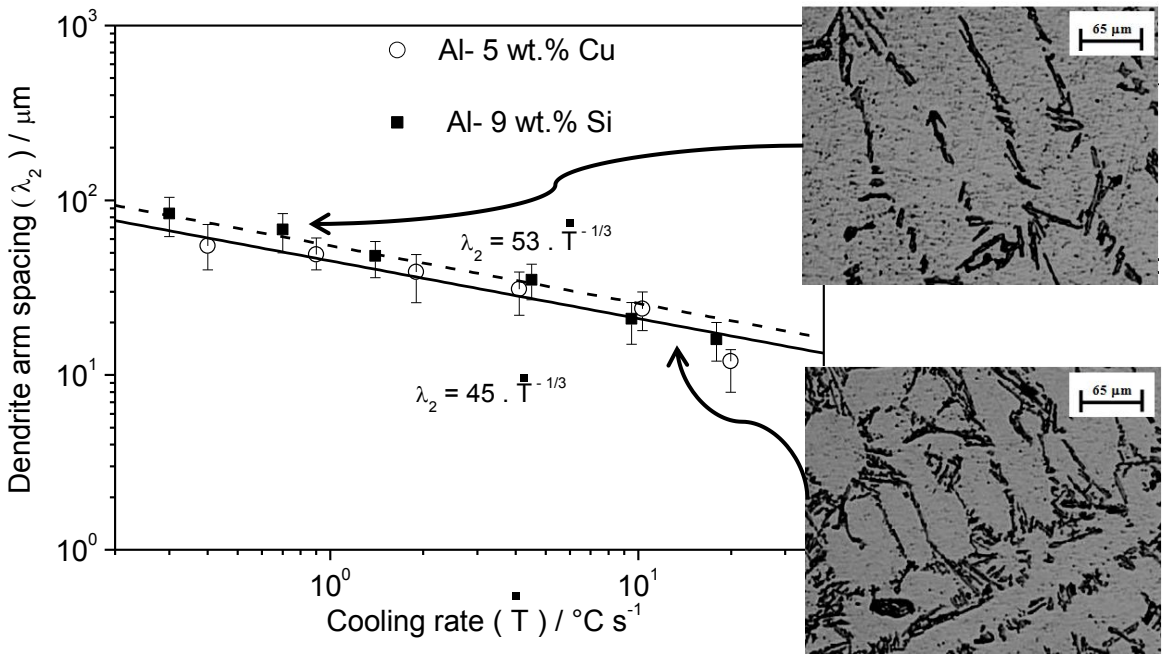

A

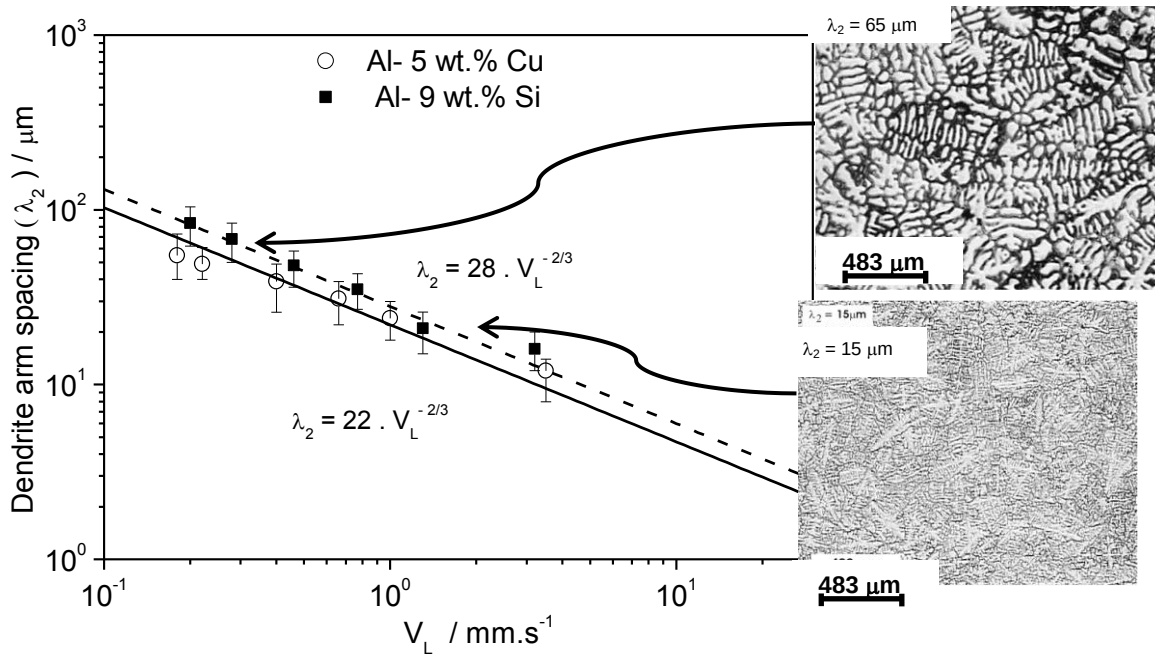

B

Figure 3. Dendrite arm spacing as a function of (a) cooling rate and (b) tip growth rate, V_L for Al – 5 wt.% Cu and Al 9 wt.% Si as-cast alloys.

Such eutectic mixture nucleate in a cooperative and alternative way during growth and remains located between the dendritic arms. The resulting microstructure of the Al-Si alloy consists of an Al-rich dendritic matrix with a eutectic mixture in the interdendritic region formed by needle-like silicon crystals set in an Al-rich phase.

3.2 Dendrite arm spacing and mechanical properties

Figs. 4a and 4b depict the experimental results of UTS-ultimate tensile strength (σ_U) and YS-yield strength (0.2% proof stress; $\sigma_{y=0.2}$) as a function of the secondary dendrite arm spacing (λ_2), for the Al 5 wt.% Cu and Al 9 wt.% Si alloys, respectively. It can be seen that for both alloys the UTS increases with the decrease in the secondary dendrite arm spacing. It is important to emphasize that the 0.2 % proof stress do not strictly represent the limit between elastic and plastic tensile properties. The improvement of strength by a reduction in λ_2 seems to be the result of the number of separate effects, all of which seem to operate beneficially. Slight faults during growth will cause the dendrite arms within a grain to become slightly misoriented, and the higher the degree of misorientation, the greater the resistance will be to the passage of a slip plane. Other contributions to the difficulty of propagating slip across the interdendritic region include the presence of segregated solute, which would alter the local hardness by solute strengthening, and possibly by precipitation of other phases. Also there may be present macroscopic particles which may be hard and strong, so constituting effective barriers to

slip. As λ_2 is reduced, the cast structure becomes cleaner and sounder, and these qualities are important contributors to improved properties [19].

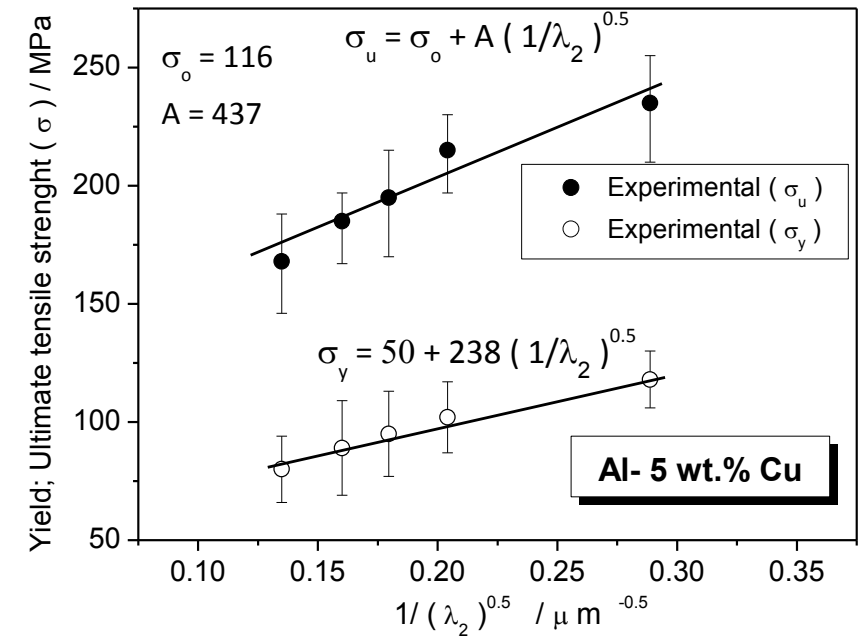

A

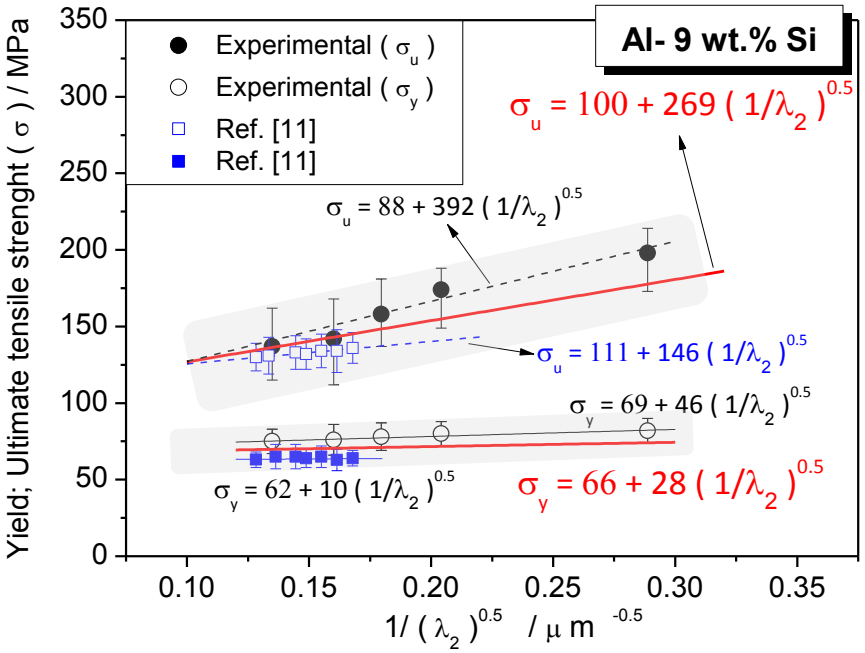

B

Figure 4. Ultimate (σ_u) and yield tensile strengths (0.2% proof stress : $\sigma_{y\,=\,0.2}$) as a function of the secondary dendrite arm spacing (λ_2) for (a) Al – 5 wt.% Cu and (b) Al 9 wt.% Si as-cast alloys

It can also be observed in Fig. 4 that the yield strength is essentially constant with the increase in secondary dendrite arm spacing for the Al-Si alloy, but increases significantly with the decrease in λ_2 for the Al-Cu alloy. A similar observation concerning the yield strength of an Al-Si alloy has also been reported in the literature [2; 11]. Comparing the previously reported results of both UTS and YS as a function of λ_2 for the Al-Si alloy [11] with those of the present investigation, it can be clearly seen that the relatively small range of experimental λ_2 results examined in the previous study do not allow a general equation relating mechanical strength with λ_2 to be established. On the other hand, the wider range of λ_2 examined in the present investigation can be associated with a number of important casting processes, permitting general equations for both UTS and YS with λ_2 (i.e. $\sigma_u = 100 + 269\ \lambda_2^{-0.5}$ and $\sigma_y = 66 + 28\ \lambda_2^{-0.5}$) to be proposed, which encompass the previously reported range of dendritic spacings [11], as shown in Fig. 4b.

It can also be mentioned that the strain in Al-Cu alloy is typical of alloys formed by two different metallic solid solutions, while the deformation in the Al-Si alloy proceeds by slip in the Al-rich matrix accomodated by progressive fracture in increasing number of silicon particles. Considering the present experimental results of tensile strength, it can be concluded that a more homogeneous distribution of the eutectic mixture for smaller spacing seems to contribute for the increase in the ultimate tensile strength. However, the increase in solidification rate has other general beneficial attributes, such as reduction in gas porosity (in the present experiments the alloys were degassed just before pouring), more refined eutectic structure (finer silicon crystals for the Al-Si alloy and finer Al_2Cu intermetallic particles for the Al-Cu alloy) and greater solute saturation.

3.3 Dendrite arm spacing and corrosion behaviour

In order to investigate the corrosion resistance (CR) on as-cast Al-Cu and Al-Si alloys as a function of the secondary dendrite arm spacing, a number of samples were collected along the casting length corresponding to positions 07, 21, 49 and 63 mm (± 2mm) from the bottom of the casting. These positions are the same that were selected to extract samples for tensile testing, as shown in Fig. 2. Using an automatic data acquisition system, the potentiodynamic polarization curves were plotted and both corrosion rate and potential were estimated by Tafel plots using both anodic and cathodic branches. The corrosion current densities were determined from the potentiodynamic polarization curves, as previously made using a number of conditions and alloys [11-15, 20-25]. It is important to remark that other electrochemical parameters using Bode and Nyquist plots can also be used to evaluate the electrochemical corrosion behaviour as a function of microstructure parameters, as previously reported [12-15, 23-25].

Fig. 5 shows potentiodynamic polarization curves and their corresponding corrosion current density as a function of the dendrite arm spacing for both as-cast Al-Cu and Al-Si alloys samples. It can be clearly observed that the Al-Si alloy presents the corrosion potential displaced toward the less noble potential side, independently of the scale of the dendrite spacing.

Considering the values of current density as a function of λ_2 for both Al-Cu and Al-Si alloys samples, two different trends are clearly observed. The Al 5 wt.% Cu alloy depicts an increase in

current density with the increase in the secondary dendrite arm spacing. On the other hand, for the Al 9 wt.% Si alloy the current density decreased with the increase in λ_2, as shown in Fig. 5b.

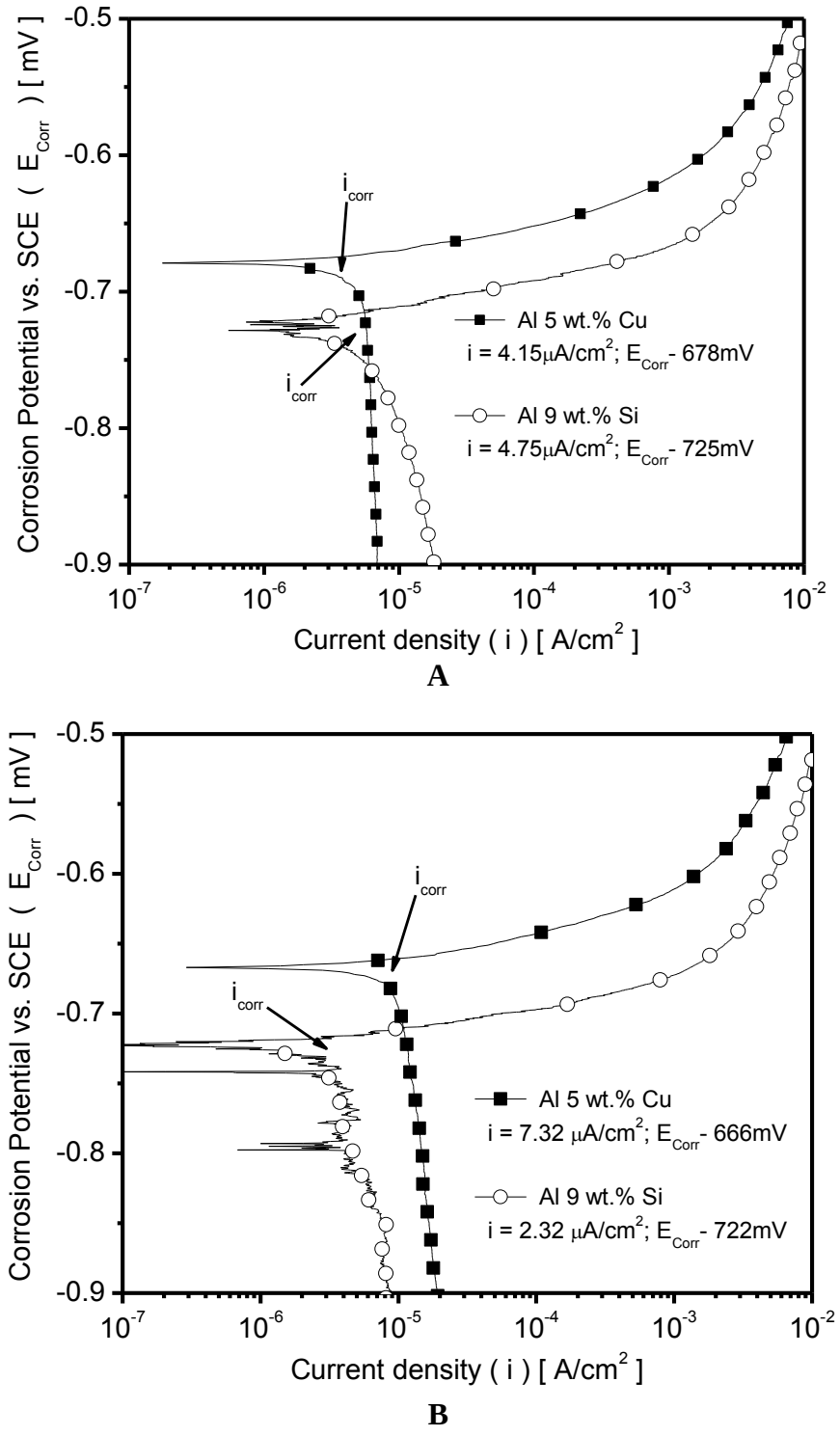

Figure 5. Experimental potentiodynamic polarization curves of Al 5 wt.% Cu and Al 9 wt.% Si alloys samples at: (a) 07 mm and (b) 63mm from the bottom of the casting.

Considering both the Al-Cu and Al-Si alloys samples with a dendritic spacing of 15μm, it can be seen that the resulting current densities are similar (about 4 to 4.5 μA x cm^{-2}). However, from this point, the Al-Cu alloy tends to have the CR increased and the Al-Si alloy the CR decreased with the increase in the secondary dendrite arm spacing (i.e. for coarse dendritic arrangements). Moreover, it will also be shown that for a secondary dendrite spacing of 15μm, the UTS of both alloys are also very similar (of about 200 MPa).

3.3.1 Corrosion behaviour of the Al-Cu alloy

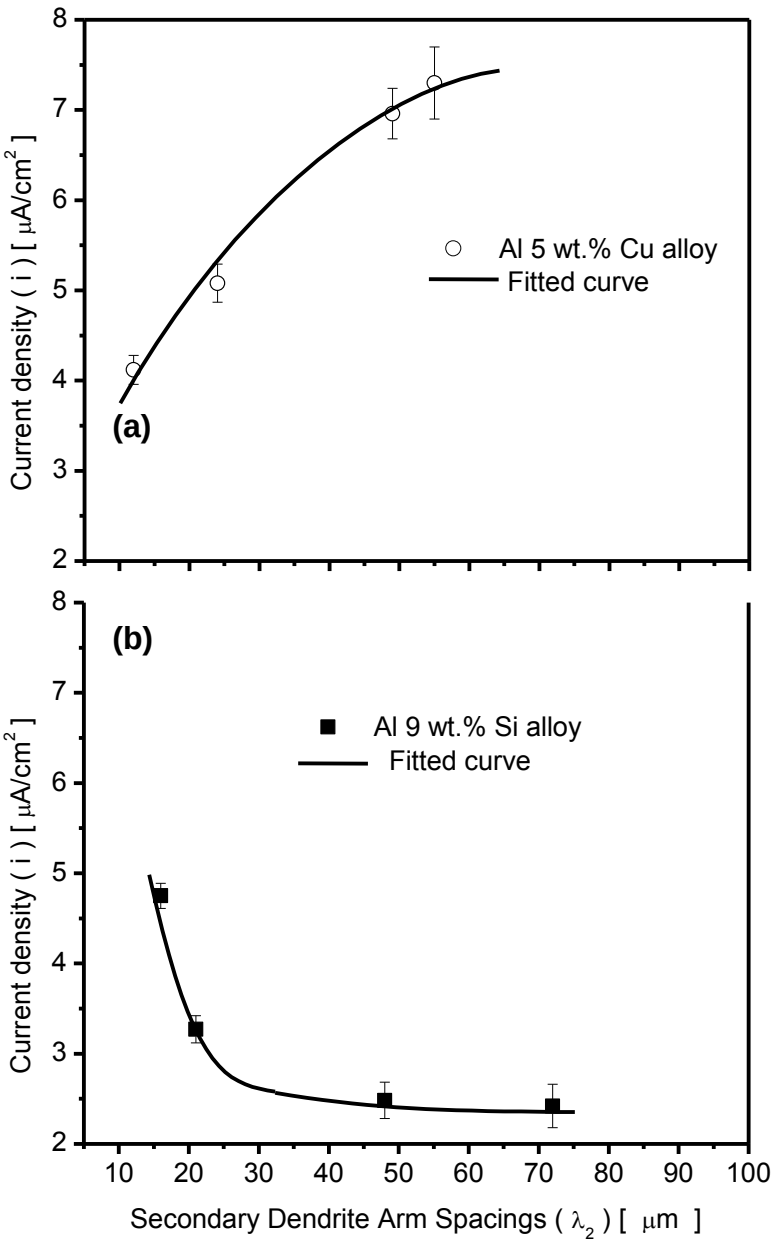

Figure 6. Experimental corrosion current density as a function of the secondary dendrite arm spacing for (a) Al 5 wt.% Cu and (b) Al 9 wt.% Si alloys.

For the Al 5 wt.% Cu, it is known that the final microstructure at room temperature will be composed of an Al-rich dendritic matrix and an interdendritic lamellar eutectic mixture containing Al_2Cu intermetallic particles, as previously reported [10, 26]. The corrosion current density for samples extracted from positions close to the bottom of the casting (finer secondary dendrite arm spacings) is lower than those of the other positions experimentally examined, as shown in Fig. 6, i.e., the corrosion resistance decreases with the increase in λ_2.

The lower corrosion resistance observed for coarser dendritic structures of the Al- 5 wt.% Cu alloy is associated with larger interdendritic regions (larger areas of Al_2Cu which are more susceptible to corrosion action). Due to the inverse segregation phenomenon, the bottom part of the casting is a relatively Cu richer region when compared with solute concentrations at regions which are closer to the casting top, as reported in a previous investigation [26]. With the higher cooling rates close to the cooled surface of the casting, finer dendritic spacings are formed and a more homogeneous distribution of Al_2Cu is attained contributing to the increase in corrosion resistance. Smaller dendritic spacings and hence smaller eutectic interphase spacing will provide a more extensive distribution of the "protective barrier". The difference in corrosion potential between the aluminum-rich phase and the intermetallic particles provides a driving force for pitting corrosion, which promotes the detachment of intermetallic particles from the alloy microstructure, as shown in Fig. 7.

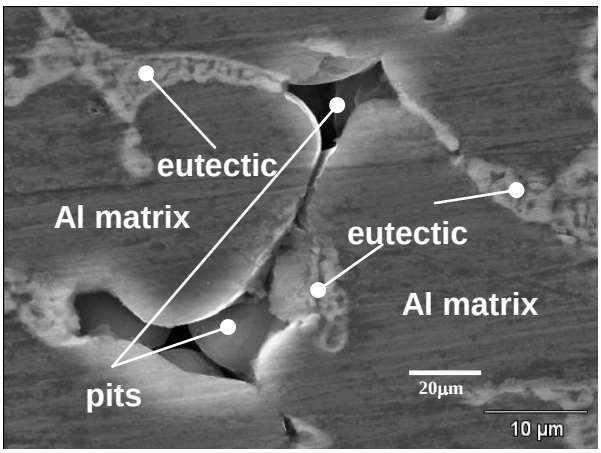

Figure 7. Typical SEM micrograph of a corroded Al 5 wt.% Cu alloy after potentiodynamic polarization test in a 0.5 M NaCl solution.

3.3.2. Corrosion behaviour of the Al-Si alloy

The analysis of the experimental results shown in Fig. 6 permits to confirm that coarser dendritic structures tend to improve the corrosion resistance of the Al 9wt%Si alloy. Considering the as-cast Al-Si alloy, the Al-rich dendritic matrix is delimited by interdendritic regions which are also constituted by a eutectic mixture, i.e., Al-rich phase and Si particles, as shown in Fig. 8.

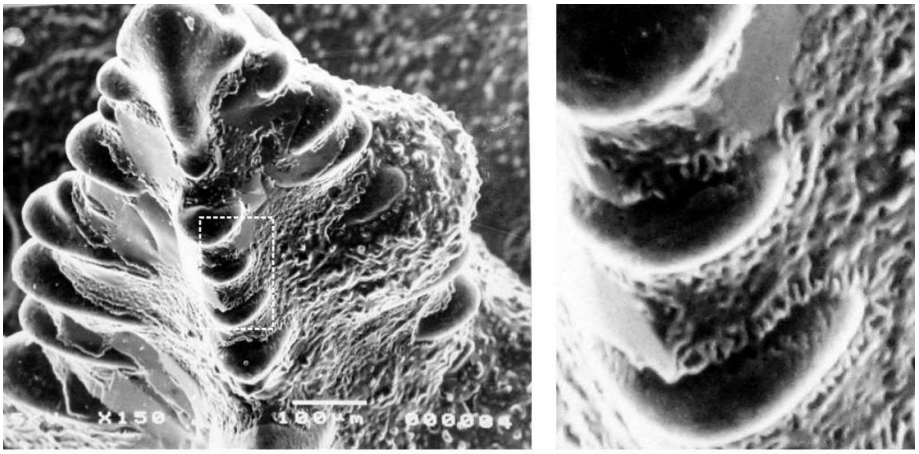

Figure 8. Typical SEM dendritic microstructure of a hypoeutectic Al-Si alloy: (a) dendritic matrix; (b) detail of secondary arm spacing and interdendritic region.

The Al-rich (α) phase and Si have dissimilar growth behavior, with Si growing from the liquid in a faceted manner (smooth growth interface) while the α phase solidifies with surfaces that are rough. Because of the different mentioned growth mechanisms of each phase, their boundaries will not be perfectly conformed, but rather will be subjected to a certain strain in the atomic level mainly on the α phase side of the contacting interface.

It seems that these regions, because of such localized strain, could be more susceptible to corrosion than α-phase regions which are not so close to the Si particles. That could explain the present experimental results, i.e., a coarser dendritic structure would exhibit a higher trend of improvement in the corrosion resistance for the Al-Si alloy since smaller dendritic spacings result equally in smaller interdendritic areas and in a more extensive distribution of silicon particles throughout the casting (thus contributing to dissemination of areas where corrosion could be initiated and develop).

3.4 Correlation between corrosion resistance and mechanical strength

Experimental results of corrosion resistance and ultimate tensile strength were combined in plots as a function of the secondary dendrite arm spacing for both Al 5 wt.% Cu and Al 9 wt.% Si alloys, as shown in Fig.9. The corrosion resistance (CR) is represented by the inverse of the experimental results of current density (i) permitting the evolution of corrosion resistance and tensile strength with λ_2 to be compared. It can be seen that for the Al-Cu alloy (Fig. 9a) the corrosion resistance and the mechanical strength exhibit a similar trend with λ_2, i.e. both decrease with the increase in the secondary spacing. However, for the Al-Si alloy (Fig. 9b) a dissimilar trend is observed, with a decrease in UTS and an increase in CR with the increase in λ_2.

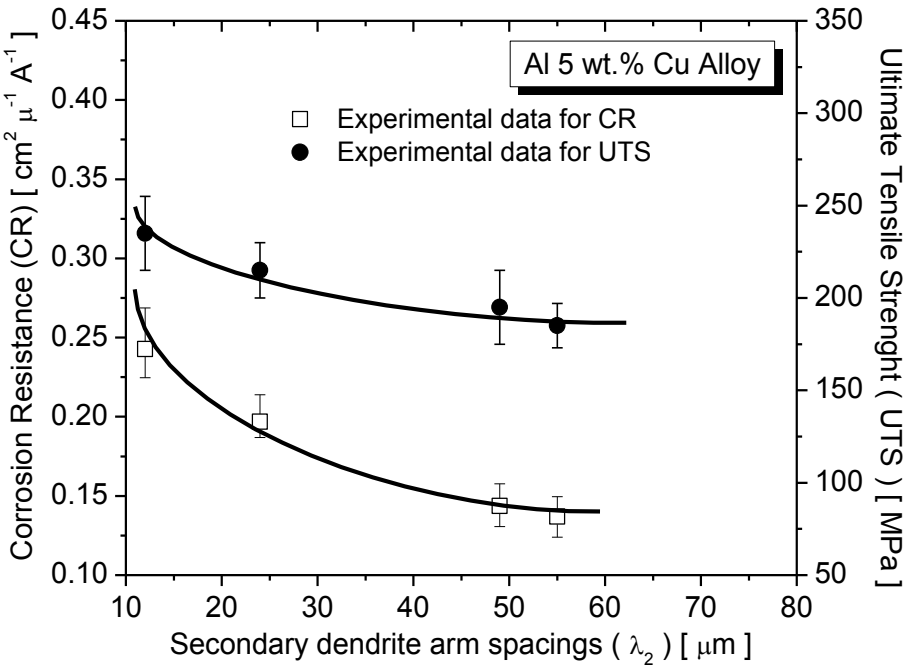

A

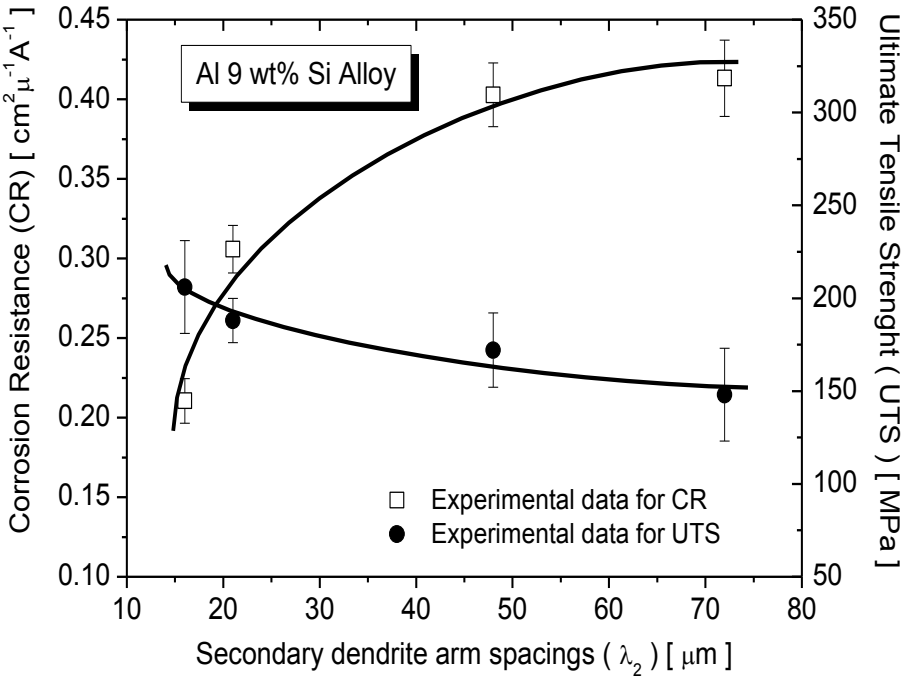

B

Figure 9. Corrosion resistance (CR) and ultimate tensile strength (UTS) as a function of the secondary dendrite spacing (λ_2) for: (a) as-cast Al 5 wt.% Cu and (b) Al 9 wt.% Si alloys

It is well known that the great challenge in engineering applications is the improvement of a property without provoking deleterious effects in another property. Thus, the aim of such combined plots is to design an "ideal" range of microstructural dendritic spacings which determines a region with

a compromise between good corrosion resistance (CR) and good tensile strength (UTS) for these alloys.

4. CONCLUSIONS

From the present experimental investigation, the following main conclusions can be drawn:

1. For both Al 5 wt.% Cu and Al 9 wt.% Si alloys the ultimate tensile strength (UTS) increases with the decrease in the secondary dendrite arm spacing (λ_2). In both cases a more homogeneous distribution of the eutectic mixture for smaller spacings seems to be responsible for the increase in tensile strength.

2. For the Al 5 wt.% Cu alloy, smaller dendritic spacings and hence smaller eutectic interphase spacings will provide a more extensive distribution of the "protective barrier" against the corrosion action. The Al_2Cu particles are enveloped by the Al-rich phase in the eutectic mixture which acts as a protection against corrosion.

3. The experimental results of potentiodynamic polarization curves have shown that coarser dendritic structures tend to yield higher corrosion resistance than finer dendritic structures for the Al 9 wt.% Si alloy. Such tendency of better corrosion resistance presented by coarser dendritic microstructures seems to be associated with the growth morphology of the two phases which constitute the interdendritic eutectic mixture.

4. A combined plot of corrosion resistance and mechanical strength as a function of λ_2 is proposed for conditions where a dissimilar behavior of such properties is observed, as it is the case of Al-Si alloys. This will permit to determine a compromise between these properties as a function of the scale of the dendritic array.

5. The control of as-cast microstructures, by manipulating solidification processing variables, permitting the control of cooling rate and tip growth rate can be used as an alternative way to produce components with a compromise between good corrosion behaviour and good mechanical properties which occurs for a specific range of dendritic arm spacings.

ACKNOWLEDGEMENTS

The authors acknowledge the financial support provided by CNPq (The Brazilian Research Council), FAEPEX UNICAMP and FAPESP (The Scientific Research Foundation of the State of São Paulo, Brazil).

References

1. E.L. Rooy. "Aluminum and Aluminum Alloys" in Castings: Metals Handbook, ASM International, Metals Park, Ohio, USA, 1988, vol. 15, pp. 743-70.
2. S. G. Shabestari and H. Moemeni. *J. Mater. Proc.Technol.*, 153/4 (2004)193
3. MIL-HDBK-5H, Military Handbook, Metallic materials and elements for aerospace vehicle structures, Chapter 3, vol. 3-1. 1998.
4. N. J. Petch. *J. Iron Steel Inst.* 174 (1953) 25

5. A.Lasalmonie and J. Strudel., *J. Mater. Sci.* 21 (1986)1837
6. D. Dubé, A. Couture, Y. Carbonneaut, M. Fiset, R. Angers and R. Tremblay. *Int. J. Cast Met. Res.*, 11 (1998) 139
7. P. Donelan. *Mater. Sci. Technol.* 16 (2000) 261
8. W. R. Osório, A. Garcia. *Mater. Sci. Eng.*, 325 (2002) 103
9. W. R. Osório, C. A. Santos, J. M. V. Quaresma, A. Garcia. *J. Mater. Proc. Technol.*, 143 (2003) 703
10. J. M. Quaresma, C. A. Santos, A. Garcia. *Metall. Mater. Trans. A*, 31 (2000) 3167
11. W.R. Osório, P.R. Goulart, G.A. Santos, C. Moura Neto, A. Garcia. *Metall. Mater. Trans. A*, 37 (2006) 2525
12. W.R. Osório, L.C. Peixoto, A. Garcia. *J. Power Sources*, 195 (2010) 1726
13. W.R. Osório, D.M. Rosa, A. Garcia. *Int. J. Electrochem. Sci.*,6 (2011) 1522
14. L.C. Peixoto, W.R. Osório, A. Garcia, *J. Power Sources*, 195 (2010) 621
15. W.R. Osório, L.R. Garcia, L.C. Peixoto, A. Garcia, *Mater. Des.*, 32 (2011) 4763
16. M.D. Peres, C.A. Siqueira, A. Garcia. *J. Alloys Compound*, 381 (2004)168
17. C. A. Siqueira, N. Cheung, A. Garcia. *Metall. Mater. Trans.A* 33(2002) 2107
18. O.L. Rocha, C.A. Siqueira, A. Garcia. *Metall. Mater. Trans. A*, 34 (2003) 995
19. J. Campbell. "Castings", Butterworth-Heinemann, Oxford, United Kingdom, pp. 264-267. 1991.
20. I.E. Castañeda, J.G. Gonzalez-Rodriguez, G. Dominguez-Patiño, R. Sandoval-Jabalera, M.A.Neri-Flores, JG. Chacon-Nava, A. Martinez-Villafañe, *Int. J. Electrochem. Sci.*, 6 (2011) 404
21. R. Lopez-Sesenes, J.G. Gonzalez-Rodriguez, M. Casales, L. Martinez, J.C. Sanchez-Ghenno, *Int. J. Electrochem. Sci.*, 6 (2011) 1772
22. F. El-Taib Heakal, A.S. Fouda, M.S. Radwan, *Int. J. Electrochem. Sci.*, 6 (2011) 3140
23. W.R. Osório, N. Cheung, L.C. Peixoto, A. Garcia, *Int. J. Electrochem. Sci.*, 4 (2009) 820
24. H .A. Barham, S. A. Brahim, Y. Rozita, K. A. Mohamed, *Int. J. Electrochem. Sci.*, 6 (2011) 181
25. J.A. Ruiz, I. Rosales, J.G. Gonzalez-Rodriguez,J. Uruchurtu, *Int. J. Electrochem. Sci.*, 5 (2010) 593
26. W.R. Osório, J.E. Spinelli, I.L. Ferreira, A. Garcia. *Electrochim. Acta*, 52 (2007) 3265